

Modeling the shadow of Sgr A* through an eclipsing black hole

Milton Jair Santibañez-Armenta,^{*} Gustavo Magallanes-Guijón,[†]

Sergio Mendoza,[‡] & Alejandro Cruz-Osorio[§]

Instituto de Astronomía, Universidad Nacional Autónoma de México, AP 70-264, Ciudad de México 04510, México

Accepted XXX. Received YYY; in original form ZZZ

ABSTRACT

The Event Horizon Telescope (EHT) observations of Sgr A* resolved the photon ring at the galactic centre, revealing a diameter of $51.8 \mu\text{as}$ (Event Horizon Telescope Collaboration et al. 2022a,b). The ring-like structure is consistent with that of a Kerr black hole. However, the source of the high bright regions in the image and the time variability remain an open question. Besides the plasma properties and emission models, the spacetime geometry also holds an important role. We present an image depicting the bright hot spots consistent with Sgr A* observations at a wavelength $\lambda = 1.3 \text{ mm}$. The image is the result of an eclipsing Schwarzschild black hole situated along the line of sight between the galactic centre and Earth. The separation from both, primary (Sgr A*) and secondary (eclipsing) black holes is 10233 AU. The central supermassive black hole located at the centre of the galaxy has an observational mass of $4.14 \times 10^6 M_{\odot}$ and the secondary eclipsing black hole has an inferred mass of $1035 M_{\odot}$.

Key words: hydrodynamics – galaxies:active – Sgr A*

1 INTRODUCTION

The galactic centre, commonly referred as Sagittarius A* (Sgr A*), has been extensively observed using various astronomical instruments across different parts of the electromagnetic spectrum (Gallego-Calvente, A. T. et al. 2021; Adams et al. 2021; Hildebrand et al. 1978). Notably, Very Long Baseline Interferometry (VLBI) techniques have allowed for a detailed imaging and characterisation of this region. Using VLBI, it has been possible to resolve a small region of the galactic centre using an extended array of telescopes called the Event Horizon Telescope (EHT) which produced a detailed image of the shadow of a supermassive black hole surrounded by an accretion flow (Event Horizon Telescope Collaboration et al. 2022a). The image clearly shows three bright hot spots around the photon ring.

In this work we report the shadow produced by the presence of a second Schwarzschild black hole located between Sgr A* and Earth. The secondary black hole with mass of $1035 M_{\odot}$, produces a lensing effect on the light beams emitted at the accretion disc around the primary supermassive black hole with mass of $4.14 \times 10^6 M_{\odot}$ and generates an eclipsed image of the Sgr A* shadow, similar to the one produced by the Event Horizon Telescope Collaboration et al. (2022b).

The first step in our modelling involves a general relativistic magnetohydrodynamics (GMHD) simulation of a Kerr black

hole spacetime with dimensionless spin parameter $a_{*} = 15/16$ and accretion disc with constant specific angular momentum $\ell = 6.76$, using the code BHAC v1.1 (Porth et al. 2017; Olivares et al. 2019). The rotating black hole has a hydrodynamic equilibrium torus surrounding it which is perturbed by a weak single-loop poloidal magnetic field defined by its inner edge $r_{\text{in}} = 20 M$ and central radius $r_c = 40 M$ (Fishbone & Moncrief 1976; Font & Daigne 2002; Shiokawa et al. 2012; Rezzolla & Zanotti 2013; Cruz-Osorio et al. 2020). The plasma is described by a relativistic gas with an ideal equation of state (see e.g. Rezzolla & Zanotti 2013), with adiabatic index $\Gamma = 4/3$.

To compute the millimetre image of the accretion flow about Sgr A* the radiative-transfer equation along null geodesics, where the electromagnetic radiation propagates (Younsi et al. 2012, 2020), is solved. We computed 500 snapshots covering $\approx 38 \text{ h}$ of observations given the estimated mass of Sgr A* of $4.14 \times 10^6 M_{\odot}$. The image size is computed adopting a distance to Sgr A* of 8.127 kpc (Event Horizon Telescope Collaboration et al. 2022a,b). The radiative transfer calculations require the use of a non-thermal energy distribution for the modelled electrons (Davelaar et al. 2018; Fromm et al. 2022; Cruz-Osorio et al. 2022; Röder et al. 2023; Zhang et al. 2024), which is a combination of a thermal electron population and of a population with a power-law energy distribution inspired by particle-in-cell simulations (cf. Ball et al. 2018; Meringolo et al. 2023; Imbrogno et al. 2024), with injection radius $r_{\text{inj}} = 10$ and the fraction of magnetic energy contributing to the heating of the radiating electrons $\varepsilon = 0.5$. The electron temperature is computed

^{*} E-mail: msantibanez@astro.unam.mx (MJSA)

[†] Email: gmagallanes@astro.unam.mx (GMG)

[‡] Email: sergio@astro.unam.mx (SM)

[§] Email: aosorio@astro.unam.mx (ACO)

using the R- β model (Mościbrodzka et al. 2009). To compute the mass accretion rate, we normalise the emission at a resolution of 600×600 pixels, which corresponds to a field of view of $150 \mu\text{s}$ in order to reproduce the observed flux of Sgr A* at 230 GHz of $\simeq 2.4 \text{ Jy}$ (Event Horizon Telescope Collaboration et al. 2022a). The resulting mass accretion rates are $\dot{M} = [1.41, 1.37, 1.32, 1.29] \times 10^{-8} M_{\odot} \text{ yr}^{-1}$, respectively. The inclination angle of the observation is assumed to be fixed at 0° , 30° , 45° , 90° , as deduced from the recent observations of the EHT (Event Horizon Telescope Collaboration et al. 2022b). Under these assumptions, only two of the hot spots in Sgr A* can be reproduced, so far, the numerical GRMHD simulations considering a single black hole have not been capable of reproducing the observed third hot spot.

In the present work we construct a model in which a secondary eclipsing black hole with a mass $\approx 1000 M_{\odot}$ at a distance of $\approx 1200 \text{ AU}$ from the primary black hole in Sgr A* is capable of bending light rays. This secondary eclipsing black hole is contained in the line of sight between the galactic centre and Earth and as shown in Figure 1 is capable of bending the original shadow of Sgr A* in such a way as to reproduce the third bright hot spot.

2 ECLIPSING BLACK HOLES

The eclipsed image was generated by a secondary Schwarzschild black hole using the recently developed numerical code *aztekas-shadows*, which evolves the geodesic equations using a 4th order Runge-Kutta method (see e.g. Sirca & Horvat 2012), solving the schematic configuration shown in Figure 1. The algorithm consists of emitting perpendicular light beams from a detector grid with the same size and resolution as that of Sgr A*'s images of 600×600 pixels, which corresponds to $150 \mu\text{s}$ field of view, located at a distance d_{obs} from the secondary black hole. Those beams are deflected by the secondary black hole and some of them would intersect the image of Sgr A* located at a distance d_{sec} from the secondary black hole, in the opposite direction of the grid. The distances d_{obs} and d_{sec} are greater than $2GM_{\text{sec}}/c^2 \times 10^4$, which is 10^4 times the gravitational radius $r_{\text{g,sec}}$ of secondary black hole, where its gravitational influence is essentially negligible (see e.g. Younsi 2014). Therefore, the plane where the image of Sgr A* is located and the detector are parallel to each other. Every light beam which intersects the image of Sgr A* was marked with the same corresponding intensity on the detector grid. The intensity was computed with the original pixels of the image of Sgr A* using a bilinear interpolation. The image obtained in the detector grid is thus the eclipsed shadow. In other words, this final image is the shadow of the shadow of Sgr A*.

We selected the best image that shows two clear and well-defined hotspots, corresponding to a supermassive black hole as described above and an inclinations angle of $i = 30^{\circ}$ between the spin axis and Earth. Then we added a secondary Schwarzschild black hole with masses $M_{\text{sec}} \in [10^2 M_{\odot}, 10^5 M_{\odot}]$, placed at various distances $d_{\text{sec}} \in [0.2 \text{ AU}, 2000 \text{ AU}]$. The distance d_{obs} from the secondary black hole to Sgr A* image was always taken with a fixed value of $r_{\text{g,sec}} \times 10^5$ for every case.

We computed $\approx 100,000$ synthetic images of the eclipsing phenomenon, by exploring different masses and loca-

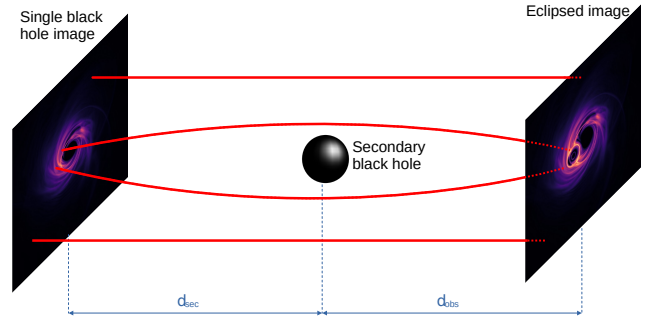


Figure 1. Artistic representation of a secondary Schwarzschild black hole with mass M_{sec} eclipsing the shadow of Sgr A*. Red lines represent light trajectories which are emitted from the single black hole image, lensed by the secondary black hole and arriving to Earth as an eclipsed image. The distances from the secondary black hole to the image of Sgr A* and the one from the secondary black hole to the camera are represented by d_{sec} and d_{obs} , respectively.

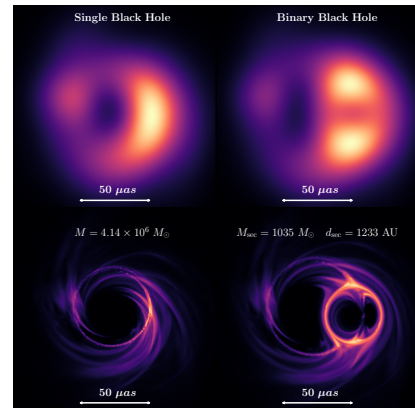


Figure 2. The left bottom panel shows the shadow of the primary Kerr black hole in Sgr A* with $a_* = 15/16$, mass $M_{\text{BH}} = 4.14 \times 10^6 M_{\odot}$ and an inclination angle of 30° with respect to the black hole spin axis. The right bottom panel is the shadow of the left bottom panel produced by an eclipsing Schwarzschild black hole. The top panels represent the blurring of their corresponding bottom images using a circular beam with radius of $20 \mu\text{s}$. The mass ratio between supermassive and the secondary black hole is $q = 2.5 \times 10^{-4}$, and the separation distance is $d_{\text{sec}} = 1233 \text{ AU}$.

tions of the secondary black hole. In particular we explored coplanar circular orbits by varying the radial direction $r \in [0 M, 15 M]$ and azimuthal position $\varphi \in [0^{\circ}, 360^{\circ}]$ around the primary black hole. In order to significantly speed up the ray-tracing process to obtain the required images, the program *aztekas-shadows* required a parallelisation procedure in its development. Using $\approx 16,000$ GPU units of an NVIDIA card with Compute Unified Device Architecture (CUDA), the computational time of the numerical simulations was reduced by five orders of magnitude.

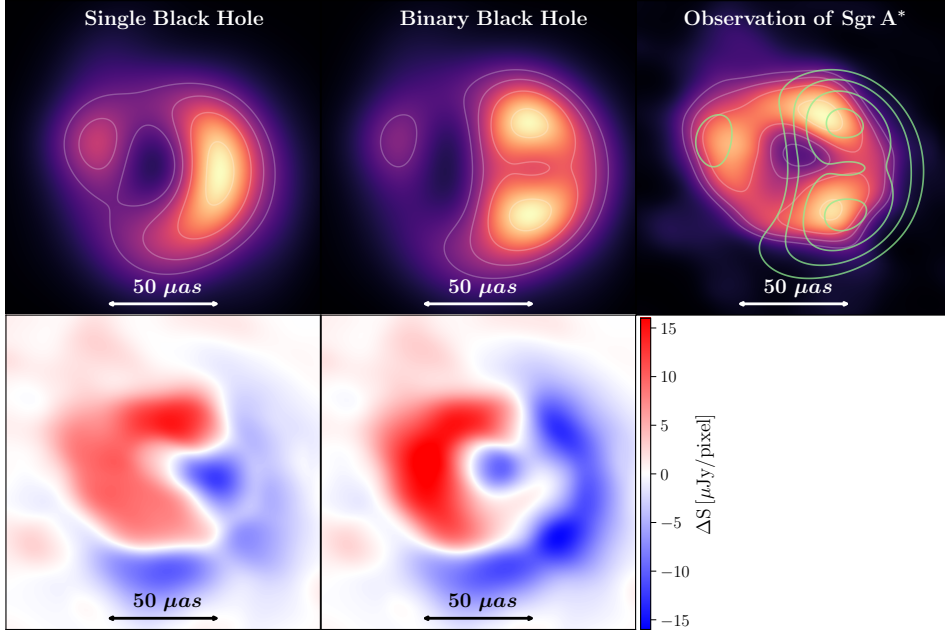


Figure 3. The top left panel shows the synthetic image a single Kerr black hole. The top middle panel is the shadow of the top left panel produced by an eclipsing Schwarzschild black hole. The top right is the observed image of Sgr A* of the EHT collaboration (Event Horizon Telescope Collaboration et al. 2022a), with green contours of the top middle image superimposed. The synthetic images were blurred using a circular beam of radio $20 \mu\text{as}$ and the white lines represent constant flux contours with values of $[2.56, 3.62, 5.12, 7.24] \times 10^{-5} \text{Jy}$. The mass of the Schwarzschild black hole is $M_{\text{BH}} = 1035 M_{\odot}$ so that the ratio between the primary to the secondary black hole is $q \approx 2.5 \times 10^{-4}$, and the separation distance between them is $d_{\text{sec}} = 1233 \text{AU}$. The bottom panels shown the relative errors between the observation of Sgr A* and the synthetic images, $\Delta S = S_{\text{obs}} - S_{\text{syn}}$.

The distances d_{sec} and d_{obs} on the eclipsed images generated by `aztekas-shadows` are much greater than the gravitation radius of the secondary black hole ($d_{\text{sec}}, d_{\text{obs}} > r_{\text{g,sec}} \times 10^3$). While, the mass of the secondary black hole $M_{\text{sec}} \lesssim 2.5 M \times 10^{-2}$ is two orders of magnitude smaller than the central supermassive black hole. Since the analysed light beams are detected practically in a perpendicular direction to the detector, their deflection angles are very small. As a consequence, a length scale l_i on the image’s grid will be modified as l_f on the image of Sgr A* so that $l_i - l_f \propto d_{\text{sec}} q$. In this way, we can reproduce similar images as long as the length-factor product $d_{\text{sec}} q$ is constant. In Figure 2, we present the accretion flow around a single black hole, producing a synthetic image with two distinct brightness regions (top-left). In contrast, the eclipsed image—resulting from the presence of a secondary black hole and representing the best-fitting model—exhibits three hot spots (top-middle), aligning well with the EHT observations (top-right). The bottom panels display the relative errors between the synthetic images and the observational data, highlighting the differences between the models.

3 SUMMARY AND CONCLUSIONS

We explored different configuration positions and masses of the secondary eclipsing black hole following the constraints imposed by Will et al. (2023). The first image of the shadow of Sgr A* was constructed numerically by considering only the supermassive black hole at the galactic centre and the emission from the magnetised accretion disc. We assumed

that the photons travel in straight paths at the distance of the secondary black hole, so that the light rays are bent when they pass near the secondary black hole. We found that the best suitable candidate to achieve the production of the third hot spot can be done by a secondary Schwarzschild black hole of mass $M_{\text{sec}} = 1035 M_{\odot}$ at a distance of $d_{\text{sec}} = 10233 \text{AU}$ from the galactic centre as shown in Figure 3. Smaller secondary black holes can also account for this third hot spot if they follow the simple analytical approximation given by $d_{\text{sec}} q \approx 0.308 \text{AU}$, where $q = M_{\text{sec}}/M$, M_{sec} is the mass of the secondary black hole and d_{sec} the separation distance between the black holes.

The synthetic image obtained from a lensed shadow image due to the presence of a secondary intermediate black hole in the galactic centre has an overall good agreement with the reconstructed average image from the EHT observations of Sgr A*. We found that the binary system with separation of 10233AU and a secondary black hole with mass of $1035 M_{\odot}$ produces a lensed image with three hot spots. Figure 3 shows a direct image comparison between the observed image of Sag A* with the numerical constructed images with and without a secondary black hole, showing that the image with a secondary black hole is a better model. Our results are also in agreement with the recent theoretical constraints of the distance and mass of the secondary compact object. The study performed by Will et al. (2023) using the Newtonian three-body problem considering the binary black hole system and the S2 star orbit found two constriction regimes for the S2 orbit not to be disrupted. The first one is when the secondary black hole is farther away than the S2 star orbit at $\sim 1020 \text{AU}$ finding that distances d_{sec} in

the range of $d_{\text{sec}} \in [1000 \text{ AU}, 4000 \text{ AU}]$ and black hole masses $M_{\text{sec}} \in [10^3 M_{\odot}, 10^5 M_{\odot}]$. The second region is inside the S2 orbit and excludes the masses for the secondary black hole in the same range, $M_{\text{sec}} \in [10^3 M_{\odot}, 10^5 M_{\odot}]$. These limits ensure that the orbit of S2 is not affected by quadrupolar perturbations and the amplitude of gravitational waves generated by the binary black holes is negligible. This means that in the search parameter space for the simulations ($d_{\text{sec}} > 1020, \text{ AU}$), a smaller value of d_{sec} requires also a smaller value of M_{sec} . Our lensed synthetic image from the binary system satisfies these constraints. Finally, in our approach, the eclipsing binary black hole could be a fly-by object or an orbiting one about the galactic centre. In the latter case for a Keplerian circular orbit, with a radius $\approx 10^4 \text{ AU}$ around the galactic centre, it would have an orbiting period of $\approx 26 \text{ yr}$. The results presented here highlight the need for further research and enhancements, particularly in modelling that incorporates the self-consistent dynamics of binary black holes surrounded by an accretion flow, and the analysis of the time variability of the light curve of Sgr A*.

ACKNOWLEDGMENTS

This work was supported by PAPIIT DGAPA-UNAM projects (IN110522, IN118325, IA103725). ACO, GMG, SM, MJSA acknowledge economic support from “Secretaría de Ciencia, Humanidades, Tecnología e Innovación” (Secihti, México), numbers: 257435, 378460, 26344, 751147. GMG and MJSA acknowledge economic support from CGEP-UNAM for a research visit at Goethe Universität, Frankfurt. ACO gratefully acknowledges “Ciencia Básica y de Frontera 2023-2024” program of Secihti (CBF2023-2024-1102).

DATA AVAILABILITY

The data that support the plots within this paper and other findings of this study are available on: <https://archive.org/details/sagAbinaryblackhole>. The public released version of the GRMHD code BHAC can be found at <https://bhac.science>. The public version or the code `aztekas-shadows` will be released soon.

REFERENCES

- Adams C. B., et al., 2021, *The Astrophysical Journal*, 913, 115
 Ball D., Sironi L., Özel F., 2018, *Astrophys. J.*, 862, 80
 Cruz-Osorio A., Gimeno-Soler S., Font J. A., 2020, *Mon. Not. R. Astron. Soc.*, 492, 5730
 Cruz-Osorio A., et al., 2022, *Nature Astronomy*, 6, 103
 Davelaar J., Mościbrodzka M., Bronzwaer T., Falcke H., 2018, *Astron. Astrophys.*, 612, A34
 Event Horizon Telescope Collaboration et al., 2022a, *Astrophys. J. Lett.*, 930, L12
 Event Horizon Telescope Collaboration et al., 2022b, *Astrophys. J. Lett.*, 930, L16
 Fishbone L. G., Moncrief V., 1976, *Astrophys. J.*, 207, 962
 Font J. A., Daigne F., 2002, *Astrophys. J.*, 581, L23
 Fromm C. M., et al., 2022, *Astron. Astrophys.*, 660, A107
 Gallego-Calvente, A. T. et al., 2021, *A&A*, 647, A110

- Hildebrand R. H., Whitcomb S. E., Winston R., Stiening R. F., Harper D. A., Moseley S. H., 1978, *Astrophys. J. Lett.*, 219, L101
 Imbrogno M., Meringolo C., Servidio S., Cruz-Osorio A., Cerutti B., Pegoraro F., 2024, *Astrophys. J. Lett.*, 972, L5
 Meringolo C., Cruz-Osorio A., Rezzolla L., Servidio S., 2023, *Astrophys. J.*, 944, 122
 Mościbrodzka M., Gammie C. F., Dolence J. C., Shiokawa H., Leung P. K., 2009, *Astrophys. J.*, 706, 497
 Olivares H., Porth O., Davelaar J., Most E. R., Fromm C. M., Mizuno Y., Younsi Z., Rezzolla L., 2019, *Astron. Astrophys.*, 629, A61
 Porth O., Olivares H., Mizuno Y., Younsi Z., Rezzolla L., Mościbrodzka M., Falcke H., Kramer M., 2017, *Computational Astrophysics and Cosmology*, 4, 1
 Rezzolla L., Zanotti O., 2013, *Relativistic Hydrodynamics*. Oxford University Press, Oxford, UK, doi:10.1093/acprof:oso/9780198528906.001.0001
 Röder J., Cruz-Osorio A., Fromm C. M., Mizuno Y., Younsi Z., Rezzolla L., 2023, *Astron. Astrophys.*, 671, A143
 Shiokawa H., Dolence J. C., Gammie C. F., Noble S. C., 2012, *Astrophys. J.*, 744, 187
 Sirca S., Horvat M., 2012, *Computational Methods for Physicists: Compendium for Students*. Graduate Texts in Physics, Springer Berlin Heidelberg, Germany, <https://books.google.com.mx/books?id=hIPip3UxX3gC>
 Will C. M., Naoz S., Hees A., Tucker A., Zhang E., Do T., Ghez A., 2023, *arXiv e-prints*, p. arXiv:2307.16646
 Younsi Z., 2014, PhD thesis
 Younsi Z., Wu K., Fuerst S. V., 2012, *Astron. Astrophys.*, 545, A13
 Younsi Z., Porth O., Mizuno Y., Fromm C. M., Olivares H., 2020, in Asada K., de Gouveia Dal Pino E., Giroletti M., Nagai H., Nemmen R., eds, Vol. 342, *Perseus in Sicily: From Black Hole to Cluster Outskirts*. pp 9–12 (arXiv:1907.09196), doi:10.1017/S1743921318007263
 Zhang M., Mizuno Y., Fromm C. M., Younsi Z., Cruz-Osorio A., 2024, *Astron. Astrophys.*, 687, A88

This paper has been typeset from a $\text{\TeX}/\text{\LaTeX}$ file prepared by the author.